JOURNAL OF SPACECRAFT AND ROCKETS
Vol. 54, No. 6, November–December 2017

Unsteady Simulations of Rocket Plume Expansions in Geostationary Earth Orbit

Andrew B. Weaver* and Iain D. Boyd†
University of Michigan, Ann Arbor, Michigan 48109-2140

DOI: 10.2514/1.A33838

Unsteady, direct simulation Monte Carlo/particle-in-cell simulations of rocket plume expansions into the magnetosphere at geostationary Earth orbit are presented for three rocket thruster pulse durations: 0.1, 1.4, and 9.9 s. The chemical rocket thruster ejects hydrazine combustion products at a mass flow rate of 4.5×10^{-4} kg/s, and the number densities is computed as a function of time for distances up to 35 km from the rocket thruster. The plume reaches steady-state operation 1 km downstream of the rocket thruster before the thruster is shut off at 1.4 s, and steady-state operation is reached as far as 20 km downstream of the rocket thruster for the 9.9 s pulse duration. An analytic expression for free molecular flow expanding into a vacuum is compared to the unsteady simulations for number densities and flow velocities, and the influences of energetic protons and electrons emitted from the sun on predicted total number densities are investigated.

Nomenclature

A_0	=	area of thruster exit, m^2
d_{ref}	=	reference diameter for variable hard sphere model, Å
$\boldsymbol{E}$	=	electric field, $V \cdot m^{-1}$
$E_{b\lambda}$	=	Planck's spectral, blackbody emissive power, $(W \cdot m^{-2})/\mu m^{-1}$
k_B	=	Boltzmann constant; 1.391×10^{-23}, $J \cdot K^{-1}$
M_w	=	species molecular weight, $kg/kmol^{-1}$
m_s	=	species mass, kg
$\dot{N}_{0,s}$	=	species number of particles ejected from the thruster exit per unit time, s^{-1}
n	=	number density, m^{-3}
n_e	=	electron number density, m^{-3}
n_r	=	index of refraction
q_0	=	elementary charge; 1.602×10^{-19}, C
T_e	=	electron temperature, K
T_{ref}	=	reference temperature for variable hard sphere model, K
$T_{0,s}$	=	species gas temperature at thruster exit, K
t_{off}	=	time when thruster is shut off, s
t_{on}	=	time when thruster is turned on, s
U_0	=	thruster exit velocity, ms^{-1}
u_r	=	radial component of velocity, ms^{-1}
u_z	=	axial component of velocity, ms^{-1}
$\boldsymbol{v}$	=	macroscopic velocity vector (u_r, u_θ, u_z), ms^{-1}
β	=	$m_s/(2k_B T_{0,s})$, s^2m^{-2}
λ	=	wavelength, μm
ϕ	=	electrostatic potential, V
ω	=	viscosity index for variable hard sphere model

Subscripts

ref	=	reference condition
s	=	species index

I. Introduction

THERE are currently over 400 satellites in geostationary Earth orbit (GEO) [1], and each satellite requires periodic firings of its rocket thrusters to maintain the proper orbit. GEO has a defined altitude of 35,786 km above sea level, which is well within the magnetosphere where high-energy particles emitted from the sun may be found. Accurate predictive capabilities for rocket plume expansions in the magnetosphere are important in order to reduce the risk of plume impingement on critical spacecraft surfaces.

The unsteady interaction between a rocket plume and the space environment at GEO is complex. Modeling the rocket plume expansion across tens of kilometers as a transient process involves 1) gas expansion into a highly rarefied gas, 2) momentum and charge exchange collisions between protons emitted from the sun and plume species, and 3) geomagnetic and electric field interactions with ions. The methodology for simulating such an environment was detailed by Stephani and Boyd [2,3]. This methodology has also been applied to the space shuttle rocket plume expansion into the ionosphere to explain the correlation between rocket firings and measured ion fluxes aboard the International Space Station [4].

Several others [5–7] have also investigated the interactions between spacecraft, rocket plumes, and the space environment, but they were focused on interactions at low Earth orbit (LEO). The lower densities, the higher energies of ambient ions, and the lower geomagnetic field strength at GEO relative to LEO change the relative importance of the various plume–atmosphere interactions; therefore, a separate analysis is required to better understand and predict plume behavior at GEO. Recently, Stephani and Boyd [8] studied spacecraft interactions with the magnetosphere with similar operating conditions, and they concluded that, unlike the ion plumes, neutral plumes were not strongly influenced by ionization mechanisms.

The aim of this work is to investigate the use of simplifying assumptions, such as no charge exchange collisions and free molecular flow, for modeling time-dependent neutral plume expansions from a rocket operated at GEO. The assumption of free molecular flow allows for the derivation of analytic expressions for flowfield properties, which are much simpler to evaluate than using a direct simulation Monte Carlo (DSMC) solver. Numerical simulations are carried out for three station-keeping maneuvers: 0.1, 1.4, and 9.9 s pulse durations using a rocket thruster with a nominal mass flow rate of 4.5×10^{-4} kg/s. Unsteady plume properties for the three station-keeping maneuvers are then compared to an analytic expression as a function of both spatial location and number flux at the thruster exit. The influences of ambient proton and electron energies on predicted plume properties are also investigated.

The remainder of the paper is organized as follows. Section II details the computational methods and collision models used to

Presented as Paper 2016-5384 at the AIAA SPACE 2016, Long Beach, CA, 13–16 September 2016; received 20 December 2016; revision received 2 May 2017; accepted for publication 10 June 2017; published online 28 July 2017.

*Postdoctoral Research Fellow, Department of Aerospace Engineering, 1320 Beal Ave. Senior Member AIAA.

†James E. Knott Professor of Engineering, Department of Aerospace Engineering, 1320 Beal Ave. Fellow AIAA.

obtain numerical predictions of neutral plume properties. Analytic formulations for unsteady, free molecular flow properties are provided in Sec. III, and time-dependent flow properties for the three station-keeping maneuvers obtained both numerically and analytically are presented in Sec. IV. Finally, concluding remarks are summarized in Sec. V.

II. Modeling of Plume/Magnetosphere Interactions

Modeling the plume interactions with the magnetosphere as it expands into the vacuum of space involves both rarefied and plasma gas dynamics. Therefore, a combination of two particle-based methods, direct simulation Monte Carlo [9] and particle in cell (PIC) [10], are employed simultaneously in the MONACO PIC (MPIC) [11] program used in this work. A description of the PIC/DSMC framework used in this work is provided in Sec. II.A, and the collision dynamics are described in Sec. II.B. The computational geometry and numerical parameters are described in Sec. II.C.

A. Particle-in-Cell/Direct Simulation Monte Carlo Framework

The DSMC method [9] is used to model the motion and collisions of neutral particles, and the PIC method [10] is used to model the charge exchange (CEX) collisions and ion acceleration due to electrostatic and magnetic fields. Bird's no-time-counter method [9] is used to model the collision frequency, and particles are moved according to standard DSMC procedures. In the case of ions, an extra step is introduced before the particles are moved to compute the acceleration due to electrostatic and magnetic fields.

Although standard PIC simulations [10] model the electrons as particles, here, the neutrals and ions are instead tracked with the electrons modeled as a fluid. Thus, the assumption of a Boltzmann energy distribution for the electron energy has been made, with the electrons equilibrated at a temperature T_e. This assumption greatly reduces the required computational resources because tracking electrons requires a much smaller time step than is used for ions [12]. By further assuming ideal, isothermal electron flow; quasi neutrality; and negligible influence of the magnetic field on the electron momentum equation, the electrostatic potential may be related to the electron number density through the Boltzmann relation:

$$\phi = \phi_{\text{ref}} + \frac{k_B T_e}{q_0} \ln\left(\frac{n_e}{n_{e,\text{ref}}}\right) \tag{1}$$

The electron number densities n_e are obtained in this PIC/DSMC framework from tracked ion number densities n_i because $n_e \approx n_i$ due to the quasi-neutrality assumption.

The acceleration due to the electric field is then obtained from the gradient of the electrostatic potential:

$$\boldsymbol{E} = -\nabla\phi \tag{2}$$

The influence of the Earth's magnetic field at GEO on the ions is modeled using the magnetic field model described by Stephani and Boyd [2,3].

B. Collision Dynamics

The hydrazine rocket thruster exhausts into high-energy electrons and H^+ ions. Assuming complete combustion, the rocket thruster combustion forms the products H_2, N_2, and NH_3. Therefore, there are three types of collisions considered in this work corresponding to momentum exchange between neutrals, momentum exchange between an ion and a neutral, and charge exchange. The redistribution of energy to internal energy modes of the colliding particles is ignored because the primary interest is in neutral number densities.

The momentum exchange between neutrals is modeled using the variable hard sphere (VHS) model [9], with the VHS model parameters listed in Table 1.

Elastic collisions between ions and neutrals result in highly forward scattering. At the relatively high energies considered in this work (1000 eV), the scattering angles are low [13,14], and therefore it is assumed that all such collisions result in complete forward scattering.

Table 1 VHS model parameters used for the plume neutral species

Species	T_{ref}, K	d_{ref}, Å	ω
H_2	273	2.92	0.75
N_2	273	4.17	0.75
NH_3	273	5.94	0.75

The third type of collision considered in this work is charge exchange. These reactions are of the type $A^+ + B \rightarrow A + B^+$; if species A is different from species B, then the charge exchange is nonresonant and involves an energy change. Most of the CEX collisions will require energy to proceed because the most frequent CEX collision is between the ambient H^+ ions and H_2 from the plume. Cross-sections for CEX collisions between H^+–H_2 and H^+–N_2 are obtained from Kusakabe et al. [15] and Lindsay and Stebbings [16], respectively. No data have been found for the CEX cross-section between H^+ and NH_3, and therefore it is assumed to have the same cross section as N_2. For the same reason, the scattering angles and direct transfer collision cross sections are assumed to all correspond to that of H^+–N_2, as reported by Cabrera-Trujillo et al. [14].

Photons emitted from the sun have sufficient energy to ionize neutral H_2 molecules, but they rarely collide to have much effect on the plume properties. The collision frequency may be computed by integrating the product of the solar blackbody emissive power to the photon energy ratio and the nondissociative H_2 photoionization cross-section from Liu and Shemansky [17]:

$$\begin{aligned}\nu &= \int_0^\infty \frac{E_{b\lambda}}{hc_0/\lambda}\sigma_I(hc_0/\lambda)\,\mathrm{d}\lambda \\ &= \frac{2\pi c_0}{n_r^2}\int_0^\infty \frac{\sigma_I(hc_0/\lambda)}{\lambda^4[\exp(hc_0/n_r\lambda k_B T)-1]}\,\mathrm{d}\lambda\end{aligned} \tag{3}$$

The radiation is in the magnetosphere where the density is very low, and therefore a value of one is used for the index of refraction n_r to calculate the nondissociative H_2 photoionization collision frequency of 1.8×10^{-6} s^{-1}. The nondissociative photoionization process for H_2 is more likely than dissociative, Compton, or double ionization [18], but its collision frequency of 1.8×10^{-6} s^{-1} is less than that of CEX collisions. Because the effect of CEX collisions on the neutral number density will be shown in Sec. II.D to be less than 7%, the effects of H_2 photoionization would also be less, and are therefore neglected.

C. Computational Geometry and Numerical Parameters

The plume flow is simulated in MPIC on the two-dimensional axisymmetric grid shown in Fig. 1, with the rocket thruster placed on the center of the axis of symmetry. The 0.9 N rocket thruster exhausts the combustion products H_2, N_2, and NH_3 in the +Z direction toward the outer computational boundary placed 35 km downstream. The

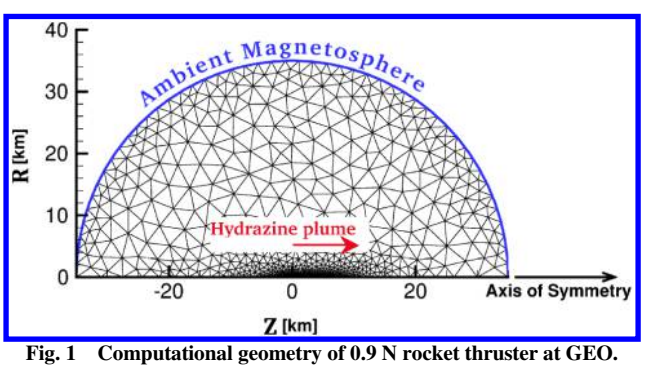

Fig. 1 Computational geometry of 0.9 N rocket thruster at GEO.

Table 2 Ambient and rocket nozzle exhaust conditions

Species	M_w, kg/kmol^{-1}	k_BT/q_0, eV	U_0, km/s	n, m^{-3}	$\dot{N}_{0,s}$, s^{-1}
H^+	1.01	1.00×10^3	0	3.00×10^6	0
H_2	2.02	0.03	1.91	2.42×10^{23}	1.24×10^{22}
N_2	28.0	0.03	1.91	1.35×10^{22}	6.82×10^{21}
NH_3	17.0	0.03	1.91	5.79×10^{22}	2.92×10^{21}

geomagnetic field lines are oriented perpendicular to the thrust vector, or in the R direction, and the magnetic field strength was reported by Chulliat et al. [19] to be 1.1×10^{-7} T.

A total of four ambient H^+ ions are randomly positioned in each cell with energies sampled from the Boltzmann distribution at 1 keV. To maintain the ambient number density of 3×10^6 m^{-3}, the particle weights are allowed to vary according to cell size. These ambient particles are not moved and do not change velocity or charge as a result of momentum or charge exchange collisions, respectively. These procedures are employed in order to ensure a sufficient number of collisions with the ambient H^+ ions occurring in this low-density environment. The assumption that H^+ ions do not deplete is weak near the thruster, where the number of H^+–H_2 collisions is the highest. Therefore, the effects of CEX collisions on the prediction of neutral plume properties are expected to be slightly exaggerated. The properties of the plume species at the rocket exhaust are assumed to be constant across the nozzle exit and are applied as boundary conditions to the simulation. The rocket nozzle exhaust and ambient ion conditions are detailed in Table 2.

In Table 2, M_w is the species molecular weight, U_0 is the thruster exit velocity, and $\dot{N}_{0,s}$ is the species number of particles ejected from the thruster exit per unit time. The values of $\dot{N}_{0,s}$ reported in Table 2 are obtained from the product of the thruster exit area and the number flux [20]:

$$\dot{N}_{0,s} = A_0 n \int_0^\infty \int_0^{2\pi} \int_0^\infty u_z f(u_z, u_\theta, u_r)\,\mathrm{d}u_z\,\mathrm{d}u_\theta u_r\,\mathrm{d}u_r = \frac{A_0 n}{2\sqrt{\beta\pi}}\left[\exp(-\beta U_0^2) + \sqrt{\beta\pi}U_0(1+\mathrm{erf}[\sqrt{\beta}U_0])\right] \quad (4)$$

Samples are averaged over 1000 time steps in order to obtain an unsteady solution of the plume expansion into the low-density H^+ flow. The time step is 0.1 ms; therefore, the averages correspond to a 0.1 s interval.

III. Unsteady Free Molecular Flow from a Point Source

Exact, analytic solutions exist for flows in the limit of free molecular flow and no external forces. In the literature [9], flows are classified as free molecular if the ratio of the mean free path to the characteristic length (λ/L) is greater than 10. This ratio is known as the Knudsen number Kn and, for the plume expansion flow in consideration, the Knudsen number defined with respect to the rocket nozzle diameter increases from about seven, 1 km downstream of the thruster, to over 1000, 35 km downstream of the thruster. Thus, it is worthwhile to formulate an analytic expression for number densities in an unsteady, free molecular flow, which may be used for comparison with MPIC simulations.

The formulation for the unsteady, free molecular flow in the absence of external forces begins with the Boltzmann equation for a single species [9,21]:

$$\frac{\partial f}{\partial t} + \boldsymbol{v}\cdot\frac{\partial f}{\partial \boldsymbol{x}} + \boldsymbol{F}\cdot\frac{\partial f}{\partial \boldsymbol{v}} = Q(\boldsymbol{x},t;\boldsymbol{v}) + J(\boldsymbol{x},t) \quad (5)$$

Assuming no external forces and no collisions, the third term on the left-hand side and the collision operator term $J(\boldsymbol{x},t)$ on the right-hand side are zero. The source term $Q(\boldsymbol{x},t;\boldsymbol{v})$ is introduced to account for the flux of particles ejected from the thruster exit. The formulation follows from Narasimha [21], where the velocity distribution function may be expressed as

$$f(\boldsymbol{x},t;\boldsymbol{v}) = f_0(\boldsymbol{x};\boldsymbol{v}) + \int_0^t Q[\boldsymbol{x}-\boldsymbol{v}(t-s),s;\boldsymbol{v}]\,\mathrm{d}s \quad (6)$$

and f_0 is the initial velocity distribution function at a time of $t=0$ s. For the case of no flow before the start of the station-keeping maneuver, f_0 is zero everywhere.

At sufficiently large distances from the rocket nozzle, the flow from the nozzle would appear to be originating from a point. The focus of this work is on the far field, which is located at least 1 km downstream of the rocket nozzle; therefore, a point source is a reasonable assumption. A point-source flow may be assumed by representing the source flow as a product of Dirac delta functions and the biased Maxwellian velocity distribution function:

$$Q(\boldsymbol{x},t;\boldsymbol{v}) = \delta(\boldsymbol{x})\dot{N}_0(t)Ku_z(\beta/\pi)^{3/2}\exp[-\beta\{(u_z-U_0)^2+u_r^2\}] \quad (7)$$

The normalization constant K is obtained from the integration of the velocity distribution function over all velocity space:

$$K = \left\{\int_0^\infty\int_0^{2\pi}\int_0^\infty u_z\exp[-\beta((u_z-U_0)^2+u_r^2)]\,\mathrm{d}u_z\,\mathrm{d}u_\theta u_r\,\mathrm{d}u_r\right\}^{-1} = \frac{2\beta}{\pi}\left\{\sqrt{\frac{\pi}{\beta}}U_0(1+\mathrm{erf}[\sqrt{\beta}U_0]) + \frac{\exp[-\beta U_0^2]}{\beta}\right\}^{-1} \quad (8)$$

where it has been assumed that the mean thruster exit velocity is only in the +Z direction with a magnitude equal to U_0.

Moments of the distribution function, such as number density and velocity, may be obtained through integration over all velocity space:

$$n(\boldsymbol{x},t) = \int_0^\infty\int_0^{2\pi}\int_0^\infty f(\boldsymbol{x},t;\boldsymbol{v})\,\mathrm{d}u_z\,\mathrm{d}u_\theta u_r\,\mathrm{d}u_r \quad (9)$$

$$\boldsymbol{v}(\boldsymbol{x},t) = \frac{1}{n(\boldsymbol{x},t)}\int_0^\infty\int_0^{2\pi}\int_0^\infty \boldsymbol{v}f(\boldsymbol{x},t;\boldsymbol{v})\,\mathrm{d}u_z\,\mathrm{d}u_\theta u_r\,\mathrm{d}u_r \quad (10)$$

Assuming that the flow is instantaneously turned on and off, as is assumed in the MPIC simulations, the time-dependent number of particles introduced at the thruster exit may be expressed as a product of the Heaviside step function: $\dot{N}_{0,s}(t) = \dot{N}_{0,s}H(t)$. This greatly simplifies the integrations in Eqs. (9) and (10) such that the number density may now be expressed as

$$n_{\mathrm{on},s}(\boldsymbol{x},t) = \mathrm{H}(t-t_{\mathrm{on}})\frac{K\dot{N}_{0,s}z}{4\beta^{3/2}(R^2+Z^2)^{5/2}} \times\exp(-\beta U_0^2)\left\{\sqrt{\pi}(Z^2(2\beta U_0^2+1)+R^2)\exp\left[\beta\frac{Z^2U_0^2}{Z^2+R^2}\right]\right. \times\mathrm{erf}c\left[\frac{\sqrt{\beta}((Z^2+R^2)/(t-t_{\mathrm{on}})-zU_0)}{\sqrt{Z^2+R^2}}\right]2\sqrt{\beta(Z^2+R^2)} \times\left.\left(\frac{Z^2+R^2}{t-t_{\mathrm{on}}}+ZU_0\right)\exp\left[-\beta\frac{Z^2+R^2}{(t-t_{\mathrm{on}})^2}-\frac{2ZU_0}{t-t_{\mathrm{on}}}\right]\right\} \quad (11)$$

A pulse may be modeled by adding

$$n_{\mathrm{off},s}(\boldsymbol{x},t) = -H(t-t_{\mathrm{off}})\frac{K\dot{N}_{0,s}Z}{4\beta^{3/2}(Z^2+R^2)^{5/2}} \times\exp(-\beta U_0^2)\left\{\sqrt{\pi}(Z^2(2\beta U_0^2+1)+R^2)\exp\left[\beta\frac{Z^2U_0^2}{Z^2+R^2}\right]\right. \times\mathrm{erf}c\left[\frac{\sqrt{\beta}((Z^2+R^2)/(t-t_{\mathrm{off}})-ZU_0)}{\sqrt{Z^2+R^2}}\right]2\sqrt{\beta(Z^2+R^2)} \times\left.\left(\frac{Z^2+R^2}{t-t_{\mathrm{off}}}+ZU_0\right)\exp\left[-\beta\frac{Z^2+R^2}{(t-t_{\mathrm{off}})^2}-\frac{2ZU_0}{t-t_{\mathrm{off}}}\right]\right\} \quad (12)$$

to the number density in Eq. (11) after the thruster is shut off at a time of $t = t_{\text{off}}$. Multiple pulses may also be modeled in this manner by expressing the species number density as a summation of all M pulses:

$$n_s(\boldsymbol{x}, t) = \sum_i^M (n_{\text{on},s,i}(\boldsymbol{x}, t) + n_{\text{off},s,i}(\boldsymbol{x}, t)) \tag{13}$$

The total number density for the entire plume is then equal to the sum of all the species number densities computed from Eq. (13):

$$n(\boldsymbol{x}, t) = \sum_s n_s(\boldsymbol{x}, t) \tag{14}$$

Velocities are similarly obtained from the integral in Eq. (10):

$$\begin{aligned} u_{Z,\text{on},s}(\boldsymbol{x}, t) &= H(t - t_{\text{on}}) \frac{K\dot{N}_{0,s} Z^2}{4n_{\text{on},s}(\boldsymbol{x}, t)\beta^2 (Z^2 + R^2)^{7/2}} \\ &\times \exp(-\beta U_0^2) \Bigg\{ \sqrt{\pi\beta} Z U_0 (Z^2(2\beta U_0^2 + 3) + 3R^2) \\ &\times \exp\left[\beta \frac{Z^2 U_0^2}{Z^2 + R^2}\right] \text{erf}c\left[\frac{\sqrt{\beta}((Z^2 + R^2)/(t - t_{\text{on}}) - Z U_0)}{\sqrt{Z^2 + R^2}}\right] \\ &\times 2C\sqrt{Z^2 + R^2} \times \exp\left[-\beta \frac{Z^2 + R^2}{(t - t_{\text{on}})^2} - \frac{2Z U_0}{t - t_{\text{on}}}\right] \Bigg\} \end{aligned} \tag{15}$$

$$\begin{aligned} u_{R,\text{on},s}(\boldsymbol{x}, t) &= H(t - t_{\text{on}}) \frac{K\dot{N}_{0,s} Z R}{4n_{\text{on},s}(\boldsymbol{x}, t)\beta^2 (Z^2 + R^2)^{7/2}} \\ &\times \exp(-\beta U_0^2) \Bigg\{ \sqrt{\pi\beta} Z U_0 (Z^2(2\beta U_0^2 + 3) + 3R^2) \\ &\times \exp\left[\beta \frac{Z^2 U_0^2}{Z^2 + R^2}\right] \text{erf}c\left[\frac{\sqrt{\beta}((Z^2 + R^2)/(t - t_{\text{on}}) - Z U_0)}{\sqrt{Z^2 + R^2}}\right] \\ &\times 2C\sqrt{Z^2 + R^2} \times \exp\left[-\beta \frac{Z^2 + R^2}{(t - t_{\text{on}})^2} - \frac{2Z U_0}{t - t_{\text{on}}}\right] \Bigg\} \\ &= u_{Z,\text{on},s} \frac{R}{Z} \end{aligned} \tag{16}$$

with the factor C defined as

$$C = \beta \left[\frac{Z^4 + R^4 + 2Z^2R^2}{(t - t_{\text{on}})^2} + U_0 \frac{Z^3 + Z^2}{t - t_{\text{on}}} + Z^2 U_0^2\right] \tag{17}$$

The velocities after the thruster is shut off are simply the opposites of the velocities during the pulse in Eqs. (15) and (16), with time t_{on} replaced with t_{off}. Thus, the velocities may be obtained for each species as a summation of all M pulses:

$$\boldsymbol{v}_s(\boldsymbol{x}, t) = \sum_i^M (\boldsymbol{v}_{\text{on},s,i}(\boldsymbol{x}, t) + \boldsymbol{v}_{\text{off},s,i}(\boldsymbol{x}, t)) \tag{18}$$

IV. Results

The 0.9 N rocket thruster is initialized at a time of $t = t_{\text{on}} = 0$ s, with the conditions listed in Table 2; and the flowfield is the ambient H^+ flow. The rocket thruster is then switched off at times of $t_{\text{off}} = 0.1$ s, $t_{\text{off}} = 1.4$ s, and $t_{\text{off}} = 9.9$ s. The total number densities are computed at 0.1 s intervals and extracted at locations (1 km, 10 deg), (5 km, 10 deg), (10 km, 10 deg), and (20 km, 10 deg) downstream of the rocket thruster. Locations nearer to the rocket thruster are not considered in this work because the focus is on the far-field flow properties.

A. Single Pulse, Where t_{off} is Equal to 0.1 Seconds

A peak in total number density is observable from Fig. 2 at a location 1 km downstream of the thruster, whereas two peaks may be observed at the 5 km location. These peak values are just 23 and 6% of the steady-state values for the 1 and 5 km locations, respectively. Therefore, there is insufficient time to reach steady-state operation at any of the four locations for the 0.1 s pulse.

The existence of multiple peaks in Fig. 2 for the 5 km location is due to differences in species mass. The lighter H_2 molecules travel at greater speeds than either the N_2 or NH_3 molecules, and therefore reach the 5 km location first and result in the first observed peak in number density. The second peak in number density is due to the arrival of the N_2 and NH_3 molecules.

At both locations, the analytic solution to the number density in Eq. (14) is in good agreement with the MPIC simulations: agreement is to within 5% of the peak number density. Two peaks are also observable in the analytic solution at the 5 km location, but the analytic solution predicts an initially slower decay after the thruster is shut off. Collisions cause the gas to diffuse and, due to the neglect of collision in the analytic solution, gas species remain in the computational domain for a longer duration than predicted from the analytic solutions. It may be observed from Fig. 2 that the slope of the analytic solution is greater than that of the MPIC solution at later times at both locations. The total number density predicted from the analytic solution at the 5 km location is just starting to decrease below those from the MPIC. This trend is also observed for the 1.4 and 9.9 s pulse durations. There is a time delay for when the

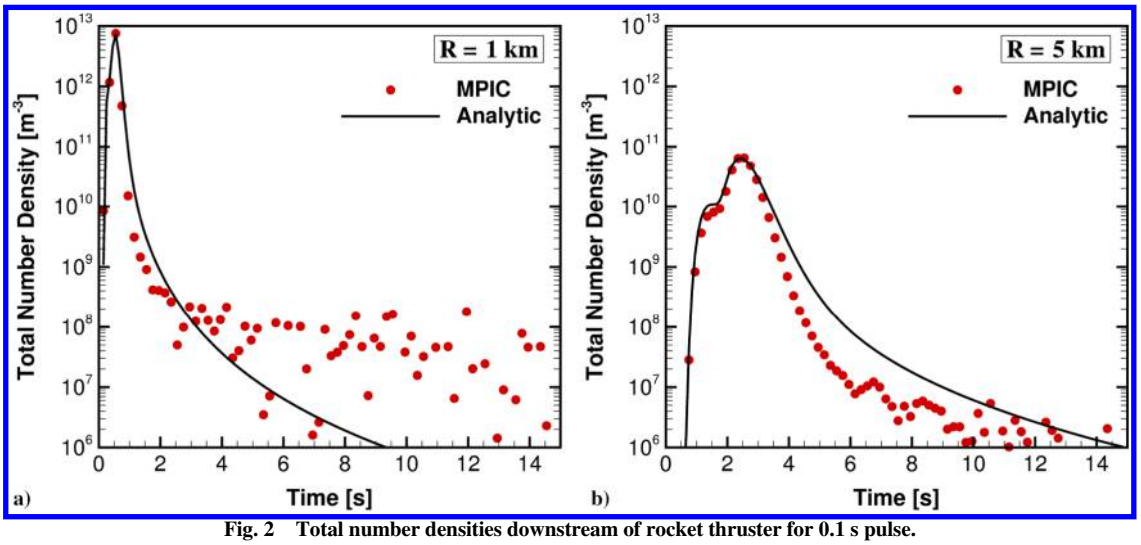

Fig. 2 Total number densities downstream of rocket thruster for 0.1 s pulse.

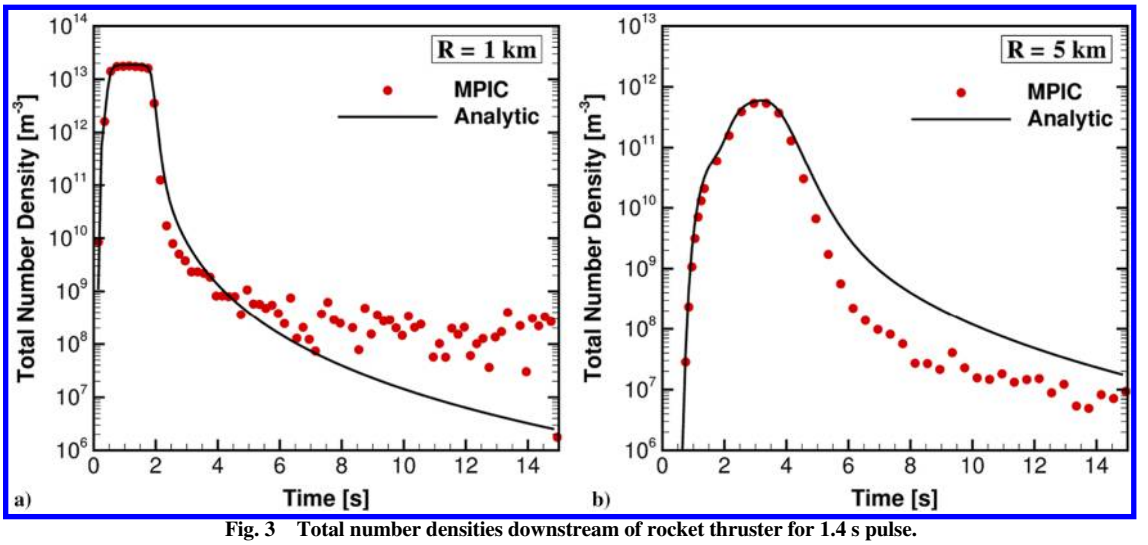

Fig. 3 Total number densities downstream of rocket thruster for 1.4 s pulse.

number densities begin to decay at farther distances downstream of the thruster due to the increase in required time to transit the distance.

B. Single Pulse, Where t_{off} is Equal to 1.4 Seconds

Increasing the pulse duration from 0.1 to 1.4 s allows sufficient time for the plume to reach steady-state operation 1 km downstream of the thruster. The peak number density is observed in Fig. 3 to plateau at 1 km, but it is 73% of the steady-state value at the 5 km location. Again, the analytic solution is in good agreement at both locations until the thruster is shut off: at which point, the effects of molecular collisions on number densities are more noticeable. The peak number density predicted by the analytic solution is within 8% of the value from the MPIC.

C. Single Pulse, Where t_{off} is Equal to 9.9 Seconds

The total number densities corresponding to electron/ion energies equilibrated at 1000 eV and with no CEX collisions are

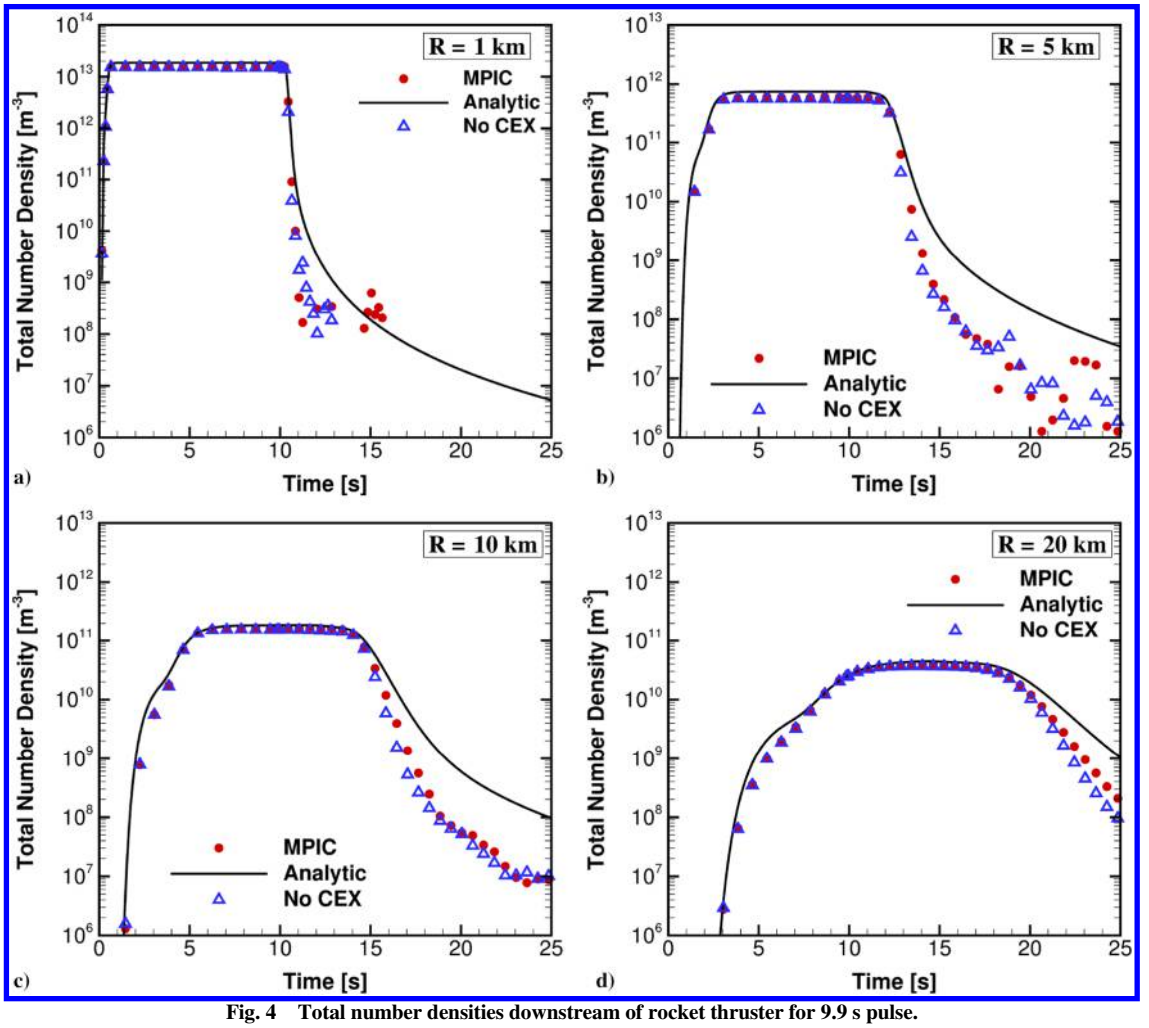

Fig. 4 Total number densities downstream of rocket thruster for 9.9 s pulse.

illustrated in Fig. 4. It is easily observable from Fig. 4 that the total number density plateaus before the thruster is shut off, and this indicates that the total number density has reached steady-state values. The total number densities at the farthest probed location of 20 km from the thruster exit are shown in Fig. 4 to approach steady state, but they do not plateau as observed at the closer locations.

The plume propagates at a finite rate; therefore, as the probed location is moved farther away from the rocket thruster, the number density plateau is shifted to later times. Also, the peak total number densities reduce by orders of magnitude as the distance from the rocket thruster is increased due to diffusion. The total number density is more than 10^{13} m^{-3} at 1 km from the thruster, but it is just 3×10^{10} m^{-3} at 20 km.

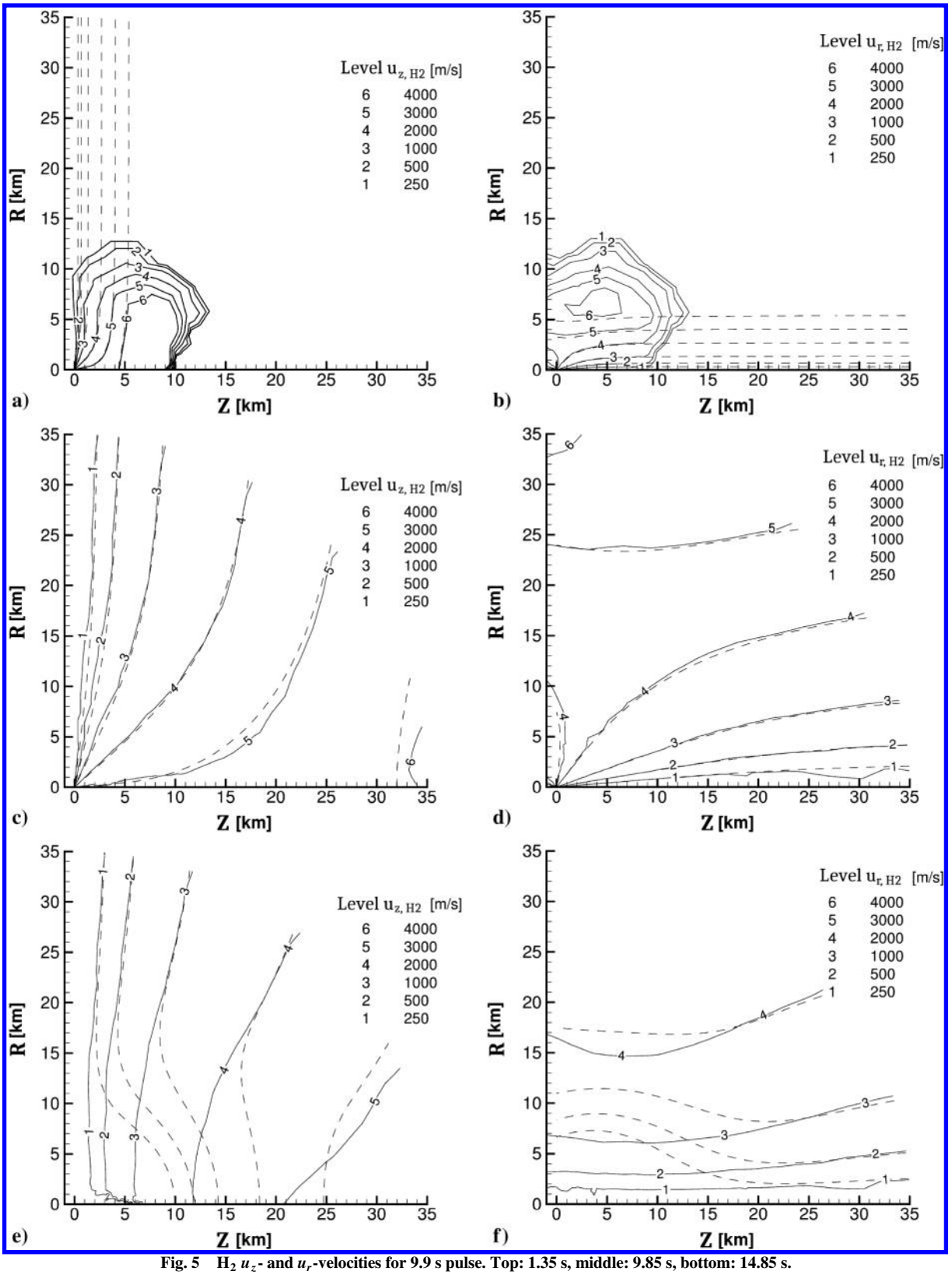

Fig. 5 H_2 u_z- and u_r-velocities for 9.9 s pulse. Top: 1.35 s, middle: 9.85 s, bottom: 14.85 s.

The total number density predictions using Eq. (14) are observed in Fig. 4 to be in good agreement with the MPIC simulations. The analytic peak number density is within 30% of the MPIC simulations with $k_B T_e/q_0 = 1000$ eV for the 1, 5, 10, and 20 km locations. This difference is due to the neglect of collisions in the analytic expression; therefore, the agreement with numerical solutions would improve with lower pressures at the thruster exit.

Agreement between the analytic solutions from Eq. (13) and from MPIC simulations also differs for each species. The agreement is best for the heaviest species, N_2; whereas the worst agreement is for the lightest species, H_2. The primary interest in this work is the neutral plume as a whole; but, comparing each individual neutral species in the plume reveals that the peak H_2 number densities tend to be as much as twice those predicted from the MPIC. The peak number densities for N_2, on the other hand, agree to within 30% of those from the MPIC, which is on the same level of agreement as the overall neutral plume.

H_2 velocity profiles obtained from Eq. (18) and MPIC simulations are shown in Fig. 5 for times of $t = 1.35$, 9.85, and 14.85 s. The agreement between the analytic solutions and the MPIC simulations is consistently better at earlier times during the pulse and at greater distances from the thruster. It may be observed from Fig. 5 that both the u_z and u_r velocities obtained from the analytic solution approach those from the MPIC simulations at large distances from the thruster.

A more quantitative comparison of the velocities may be obtained by extracting the velocities at fixed locations over a period of time, as illustrated in Fig. 6. Figure 6 shows the u_z velocities computed analytically from Eq. (18) and from MPIC simulations at locations 1, 5, and 20 km downstream of the thruster, respectively. At each location, the analytic solution lies within 3% of the MPIC simulations for the steady-state velocity. Agreement between the two solutions is noticeably better before the beginning of the plume decay at each location.

It may also be observed from Fig. 6 that the analytic solution has a much larger peak velocity shortly after the thruster is turned on. In fact, the analytic solution approaches infinity as $t \to 0$ because the number density in the denominators of Eqs. (15) and (16) approaches zero. Therefore, the analytic solution predicts unrealistically large velocities at times shortly after the thruster is turned on. However, the circular shape of the u and v velocities in Fig. 5 for the MPIC simulations at a time of $t = 1.35$ s is nonphysical. This shape implies that particles with lower velocities lead the plume, but this is not possible. The reason for the drop in velocity magnitudes at larger distances from the thruster is purely numerical; if no particles are found in a cell, then the macroscopic velocity is assumed to be zero. Agreement between the analytic solution and the MPIC simulations is best at an intermediate time after the thruster is turned on and before the decay in plume number densities begins.

D. Influence of CEX Collisions on Neutral Plume

Based on the reported electron and ion flux spectra measurements made over several solar cycles at GEO [22], the electron and ion energy distributions are found to be far from equilibrium. Thomsen et al. [22] also reported the 95% confidence interval (CI) for the flux spectra, which were then used to set the 95% CI for energy

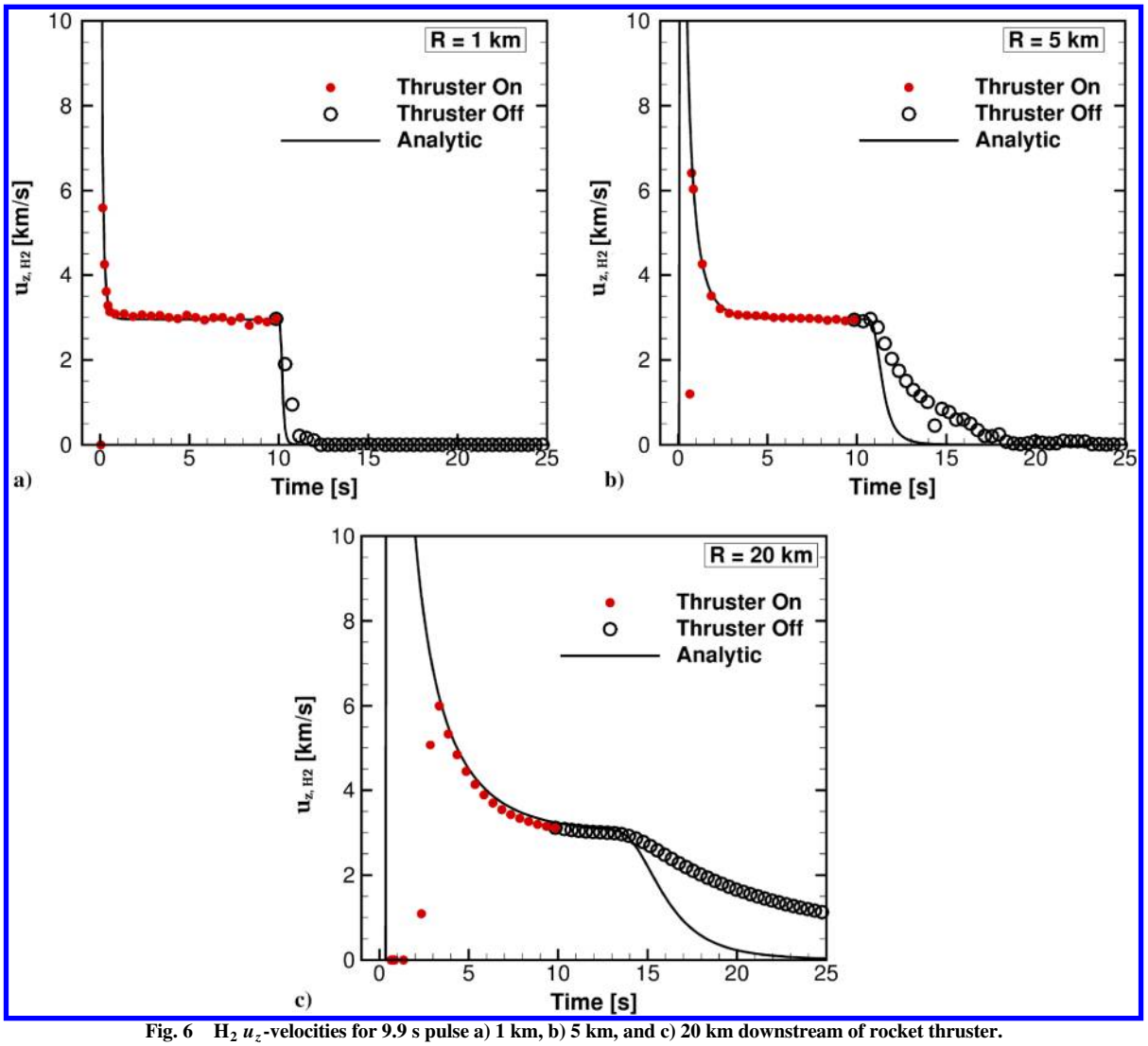

Fig. 6 H_2 u_z-velocities for 9.9 s pulse a) 1 km, b) 5 km, and c) 20 km downstream of rocket thruster.

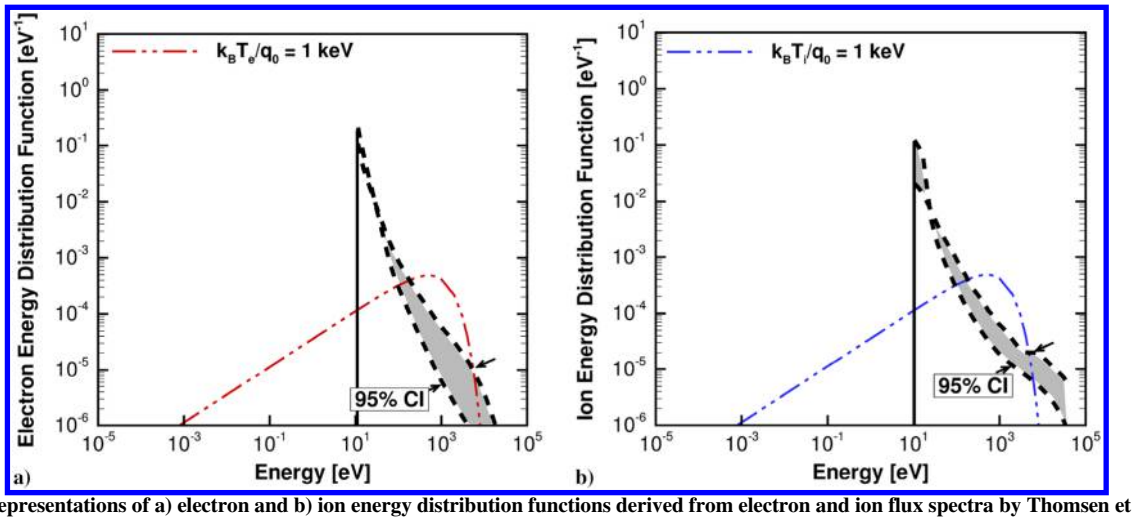

Fig. 7 Representations of a) electron and b) ion energy distribution functions derived from electron and ion flux spectra by Thomsen et al. [22].

distributions as depicted as shaded regions in Fig. 7. The $t_{off} = 9.9$ s simulations were repeated with CEX collisions being neglected.

It may be observed from Fig. 4 that the electron/ion energy energies have little influence on the peak total number densities. Up to 20 km downstream of the rocket thruster, the negligible ambient electron/ion energy results in less than 7% lower total number densities. Deviations between the two cases tend to increase shortly after the thruster is shut off, but number densities rapidly decrease towards near-ambient conditions after the thruster is shut off. This result is useful, in that it not only places a lower bound on expected number densities originating from uncertainties in ambient electron/ion energies but also helps validate the use of analytic expressions for free molecular flow with no external forces into a vacuum [21,23].

V. Conclusions

Neutral number densities have been obtained for a range of station-keeping maneuvers, and they were compared with unsteady, free molecular flow solutions. For each maneuver, the analytic solution was in good agreement with the MONACO PIC (MPIC) simulations. More noticeable differences observed between the two solutions after the thruster was shut off were due to the assumption of a free molecular flow in the analytic solution.

Velocity profiles obtained analytically are in reasonable agreement with MPIC simulations, with steady-state velocities being within 3%. This level of agreement is consistent with the agreement between total number density calculations. Velocities obtained from the analytic solution approach those from MPIC simulations far from the thruster, but the analytic solution predicts unrealistically large velocities shortly after the thruster is turned on.

Collisional effects are the most pronounced for the lightest, neutral species: H_2. Peak number densities for H_2 at each location, predicted using the analytic expression, are about twice the values predicted using the MPIC. This difference is larger than the 15–30% difference calculated for the heavier N_2 species.

Other effects, including charge exchange (CEX) collisions and nondissociative H_2 photoionization, have been determined to be negligible for neutral number density predictions. Although assuming ambient H^+ ions do not deplete is questionable, especially near the thruster, it provides a worst-case scenario for its effects on neutral number densities. The result is a mere 7% lower, peak neutral number density prediction. Molecular hydrogen is the most prevalent species and, because the photoionization collision frequency is several orders of magnitude less than that of CEX collisions, photoionization at geostationary Earth orbit would have negligible effects on the neutral plume properties.

Acknowledgments

The support of the U.S. Air Force Research Laboratory Space Vehicles Directorate and Barron Associates, Inc., for this work under subcontract FA9453-15-C-0002 is gratefully acknowledged.

References

[1] Kelso, T. S., "NORAD Two-Line Element Sets Current Data [online database]," http://www.celestrak.com/NORAD/elements/ [retrieved 28 Sept. 2015].

[2] Stephani, K. A., and Boyd, I. D., "Detailed Modeling and Analysis of Spacecraft Plume/Ionosphere Interactions in Low Earth Orbit," *Journal of Geophysical Research: Space Physics*, Vol. 119, No. 3, 2014, pp. 2101–2116.

[3] Stephani, K. A., and Boyd, I. D., "Dynamics of Spacecraft Plume / Magnetosphere Interactions in Geostationary Earth Orbit," *53rd AIAA Aerospace Sciences Meeting*, AIAA Paper 2015-1396, Jan. 2015, pp. 1–13.

[4] Stephani, K. A., Boyd, I. D., Balthazor, R. L., McHarg, M. G., Mueller, B. A., and Adams, R. J., "Analysis and Observation of Spacecraft Plume / Ionosphere Interactions During Maneuvers of the Space Shuttle," *Journal of Geophysical Research: Space Physics*, Vol. 119, No. 9, 2014, pp. 7636–7648.

[5] Mendillo, M., "Modification of the Ionosphere by Large Space Vehicles," *Advances in Space Research*, Vol. 2, No. 3, 1982, pp. 150–159. doi:10.1016/0273-1177(82)90031-X

[6] Murad, E., "Spacecraft Interaction with Atmospheric Species in Low Earth Orbit," *Journal of Spacecraft and Rockets*, Vol. 33, No. 1, 1996, pp. 131–136. doi:10.2514/3.55718

[7] Zhong, J., Zeifman, M. I., Levin, D. A., and Gimelshein, S. F., "Direct Simulation Monte Carlo Modeling of Homogenous Condensation in Supersonic Plumes," *AIAA Journal*, Vol. 43, No. 8, 2005, pp. 1784–1796. doi:10.2514/1.9566

[8] Stephani, K. A., and Boyd, I. D., "Spacecraft Plume Interactions with the Magnetosphere Plasma Environment in Geostationary Earth Orbit," *Journal of Geophysical Research: Space Physics*, Vol. 121, No. 2, Feb. 2016, pp. 1402–1412.

[9] Bird, G. A., *Molecular Gas Dynamics and the Direct Simulation of Gas Flows*, Oxford Univ. Press, New York, 1994, pp. 1–76.

[10] Birdsall, C. K., and Langdon, A. B., *Plasma Physics Via Computer Simulation*, IOP Publishing, New York, 1991, pp. 27–48.

[11] Cai, C., "Theoretical and Numerical Studies of Plume Flows in Vacuum Chambers," Ph.D. Thesis, Univ. of Michigan, Ann Arbor, MI, 2005.

[12] Serikov, V. V., Kawamoto, S., and Nanbu, K., "Particle-in-Cell Plus Direct Simulation Monte Carlo (PIC-DSMC) Approach for Self-Consistent Plasma-Gas Simulations," *IEEE Transactions on Plasma Sciences*, Vol. 27, No. 5, 1999, pp. 1389–1398. doi:10.1109/27.799817

[13] Krstic, P. S., and Schultz, D. R., "Elastic and Vibrationally Inelastic Slow Collisions: $H + H_2$, $H^+ + H_2$," *Journal of Physics B: Atomic and*

Molecular Physics, Vol. 32, No. 10, 1999, pp. 2415–2431.
doi:10.1088/0953-4075/32/10/310

[14] Cabrera-Trujillo, R., Öhrn, Y., Deumens, E., Sabin, J., and Lindsay, B., "Theoretical and Experimental Studies of the $H^+ - N_2$ System: Differential Cross Sections for Direct and Charge-Transfer Scattering at Kilo-Electron-Volt Energies," *Physical Review A: General Physics*, Vol. 66, No. 4, 2002, pp. 1–7.
doi:10.1103/PhysRevA.66.042712

[15] Kusakabe, T., Asahina, K., Gu, J. P., Hirsch, G., Buenker, R. J., Kimura, M., Tawara, H., and Nakai, Y., "Charge-Transfer Processes in Collisions of H^+ Ions with H_2, D_2, CO, and " CO_2 Molecules in the Energy Range 0.2-4.0 keV," *Physical Review A: General Physics*, Vol. 62, No. 6, 2000, Paper 62714.
doi:10.1103/PhysRevA.62.062714

[16] Lindsay, B. G., and Stebbings, R. F., "Charge Transfer Cross Sections for Energetic Neutral Atom Data Analysis," *Journal of Geophysical Research: Space Physics*, Vol. 110, No. A12213, 2005, pp. 1–10.

[17] Liu, X., and Shemansky, D. E., "Nondissociative Electron and Photon Ionization Cross Sections of Molecular Hydrogen and Deuterium," *Journal of Physics B: Atomic, Molecular and Optical Physics*, Vol. 45, No. 9, 2012, Paper 095203.
doi:10.1088/0953-4075/45/9/095203

[18] Yan, M., Sadeghpour, H. R., and Dalgarno, A., "Photoionization Cross Sections of He and H2," *Astrophysical Journal*, Vol. 496, No. 2, 1998, pp. 1044–1050.
doi:10.1086/apj.1998.496.issue-2

[19] Chulliat, A., Macmillan, S., Alken, P., Beggan, C., Nair, M., Hamilton, B., Woods, A., Ridley, V., Maus, S., and Thomson, A., "The US/UK World Magnetic Model for 2015–2020," National Geophysical Data Center, National Oceanic and Atmospheric Administration, TR, Silver Spring, MD, 2015.
doi:10.7289/V5TB14V7

[20] Bird, G. A., *Molecular Gas Dynamics and the Direct Simulation of Gas Flows*, Oxford Univ. Press, New York, 1994, pp. 77–98, Chap. 4.

[21] Narasimha, R., "Collisionless Expansion of Gases Into Vacuum," *Journal of Fluid Mechanics*, Vol. 12, No. 2, 1962, pp. 294–308.
doi:10.1017/S0022112062000208

[22] Thomsen, M. F., Denton, M. H., Lavraud, B., and Bodeau, M., "Statistics of Plasma Fluxes at Geosynchronous Orbit over More Than a Full Solar Cycle," *Space Weather*, Vol. 5, No. S03004, 2007, pp. 1–9.

[23] Cai, C., and Boyd, I., "Theoretical and Numerical Study of Free Molecular-Flow Problems," *Journal of Spacecraft and Rockets*, Vol. 44, No. 3, 2007, pp. 619–624.
doi:10.2514/1.25893

K. T. Edquist
Associate Editor